RSC Advances

PAPER

View Article Online
View Journal | View Issue

Cite this: *RSC Adv.*, 2023, **13**, 24576

On the role of functional groups in the formation of diazonium based covalent attachments: dendritic *vs.* layer-by-layer growth†

Thi Mien Trung Huynh,*[a] Kazukuni Tahara,[b] Steven De Feyter[c] and Thanh Hai Phan*[d]

Received 21st April 2023
Accepted 4th August 2023

DOI: 10.1039/d3ra02661b

rsc.li/rsc-advances

Multilayered growth is often observed upon electrografting aryl diazonium derivatives on graphitic substrates due to the reactive nature of aryl radicals. The mechanism of the multilayer formation has been investigated either by measuring the thickness of the grafted layer, the charge transfer, or *via* simulations. Spectroscopy and in particular microscopy approaches are underrepresented. Herein, we demonstrate a comparative characterization of the multilayer growth of two diazonium derivatives on highly oriented pyrolytic graphite using a combination of cyclic voltammetry, atomic force microscopy, and scanning tunneling microscopy. While dendritic growth is observed for 4-nitro phenyl diazonium (4-NBD), 4-carboxy phenyl diazonium (4-CBD) shows layer-by-layer growth upon increasing the molecular concentration, revealing the impact of the functional groups on the growth mechanism.

Introduction

Functionalizing graphene with organic molecules has attracted increasing attention due to its ability to modulate properties and widen the application of graphene in different research areas, such as molecular electronics,[1,2] catalysts and sensors,[3–5] supercapacitors and batteries,[6–8] and water splitting.[9,10] So far, two parallel approaches have been applied to modify the graphene surface: physisorption and chemisorption.[11–18] For physisorption, organic molecules randomly adsorb or self-assemble onto the graphene surface *via* weak intermolecular interactions, thereby preserving the intrinsic properties of graphene. However, these systems are usually not robust, which may limit stability against temperature and other environmental changes.[12,15,16] In contrast, chemisorption forms covalent bonds between graphene carbon atoms and molecules, thereby converting the sp^2 lattice of graphene into sp^3 lattice points at the sites attacked by the molecules.[3,6,13,17,18] These systems have been demonstrated to be more stable than physisorption but may produce more defects that detrimentally affect the novel properties of graphene.

Among the covalent functionalization approaches using organic molecules, electrochemical grafting using diazonium chemistry is the most thoroughly applied due to its speed and simplicity.[19–26] This approach relies on the electrochemical reduction of diazonium salt molecules in the vicinity of the working electrode to generate reactive aryl radicals, which subsequently bind to carbon atoms to form covalent C–C bonds, thereby permanently modifying the electronic properties of graphene. However, the degree of modification strongly depends on the quality and density of grafted molecules anchored on the graphene surface. Therefore, controlling the formation and growth of the grafted layer on the graphene surface plays a key role during the electrochemical grafting process.

It is well documented that due to their high reactivity, most aryl radicals not only attack the graphitic surfaces, but also the already grafted molecules, leading to the formation of a polyaryl layer, in cases where special strategies are not used to monitor the radical formation process.[23,27–30] This multilayered growth is influenced by several factors, including the steric and electronic effects of the aryl substituent,[31,32] solvent,[33] grafting time, and concentration of the diazonium precursor.[34] For example, the role of radical scavenger on the film growth grafted by five aryl radicals bearing different para substituents, was extensively investigated using a combination of electrochemical quartz crystal microbalance, atomic force microscopy, and X-ray photoelectron spectroscopy.[31] In the absence of a radical scavenger, all molecules form multilayers, though the extent to which depends on the functional group on the aryl group. In

[a]*Department of Chemistry, Faculty of Natural Sciences, Quy Nhon University, 170 An Duong Vuong, Quy Nhon, Vietnam. E-mail: huynhthimientrung@qnu.edu.vn*
[b]*Department of Applied Chemistry, School of Science and Technology, Meiji University, 1-1-1 Higashimita, Tamaku, Kawasaki, Kanagawa 214-8571, Japan*
[c]*Division of Molecular Imaging and Photonics, Department of Chemistry, KU Leuven, Celestijnenlaan 200F, Leuven B-3001, Belgium*
[d]*Department of Physics and Materials Science, Faculty of Natural Sciences, Quy Nhon University, 170 An Duong Vuong, Quy Nhon, Vietnam. E-mail: phanthanhhai@qnu.edu.vn*

† Electronic supplementary information (ESI) available. See DOI: https://doi.org/10.1039/d3ra02661b

addition, the influence of the electronic nature of substituent groups of aryl radicals on the grafting efficiency was also investigated by combined experimental and theoretical approaches.[32] The results suggest that the degree of functionalization electro-grafted by the radicals with electron-donating groups is higher than that of those with electron-withdrawing groups. They hypothesized the potential role of the relative position of the singly occupied molecular orbital energy levels of the aryl radicals with respect to the graphite Fermi energy level. The dependence of the number of grafted layers on the concentration of the aryl diazonium compound as well as on the scan rate, as revealed by cyclic voltammetry and X-ray photoelectron spectroscopy.[36] Accordingly, the number of layers grafted on the glassy carbon electrode was reported to vary between one and four as a function of the aryl diazonium concentration. Nevertheless, a direct observation using microscopy of the multilayer growth and the correlation of the grafting density with the diazonium aryl concentration is missing so far.

In the present work, additional insight in the mechanism of multilayer growth is reported through microscopic observations revealing that although 4-NBD and 4-CBD form similar multilayers on a graphitic surface, their grafting mechanism is different. Our findings further confirm the role of the substituent at the para position of the benzene ring of aryl diazonium salts in the mechanism of multilayered growth.

Experimental section

All scanning tunnelling microscopy (STM) experiments were conducted using a Molecular Imaging STM system, operating in constant-current mode. STM tips were prepared by mechanically cutting Pt/Ir wire (80%/20%, diameter 0.25 mm). The bias voltage refers to the substrate. For atomic force microscopy (AFM) measurements, a Multimode AFM with a Nanoscope IV controller (Veeco/Digital Instruments) was used in intermittent contact mode. Substrates consisted of highly ordered pyrolytic graphite (HOPG, grade ZYB from Advanced Ceramics Inc., Cleveland, OH). STM and AFM data analysis were performed using WSxM 5.0.[35]

4-Nitrobenzenediazonium (4-NBD) tetrafluoroborate (97%) and analytical grade hydrochloric and perchloric acid were purchased from Sigma-Aldrich and used without further purification. High purity water (Milli-Q, Millipore, 18.2 MΩ cm, TOC < 3 ppb) was used throughout. Electrolyte solutions were deoxygenated with argon gas (grade 5.0, Praxair) for several hours before use. 4-Carboxy phenyl diazonium (4-CBD) is unstable and decomposable. Therefore, it was synthesized from the aniline precursor immediately prior to electrochemical reduction. 4-Aminobenzoic acid (4-ABA) was purchased from Sigma-Aldrich and used without further purification. 4-CBD solutions with different concentrations were prepared by dissolving the desired amount of 4-ABA in HCl (50 mM); excess amount of aqueous $NaNO_2$ (0.1 M) was mixed with 5 mL amine solution approximately 3 min prior to injection into the electrochemical cell. All electrochemical measurements were performed using a VPS potentiostat (Biologic, France). Prior to each experiment, the HOPG electrode was freshly cleaved using scotch tape.

The electrochemical modification of the HOPG samples was carried out in a lab-built single-compartment three-electrode cell, with a working electrode area of 38.5 mm^2, Pt wire counter electrode, and Ag/AgCl_3M NaCl reference electrode. During the measurements, the electrolyte was kept under a solvent-saturated N_2 atmosphere. After modification, the 4-NBD and 4-CBD modified HOPG samples were rinsed with hot toluene (90 °C) followed by Milli-Q water to remove any physisorbed material from the surface and dried in a stream of N_2.

Raman measurements were performed with an OmegaScope 1000 (AIST-NT). Laser light (632.8 nm) from a He–Ne laser was focused onto the sample surface from the side (with an angle of 28° to the sample surface) and top, for "grating" and "normal" measurements, respectively, through an objective (MITUTOYO, BD Plan Apo 100, N.A. 0.7). Optical density at the sample surface was approximately 500 kW cm^{-2}. Raman scattering was collected using the same objective and directed to a Raman spectrograph (Horiba JY, iHR-320) equipped with a cooled charge-coupled device (CCD) camera (Andor Technology, DU920P-BRDD), which was operated at 100 °C. The scattering was directed through a pinhole, a dichroic mirror (Chroma Technology Corporation, Z633RDC), and a long-pass filter (Chroma Technology Corporation, HQ645LP). The accumulation time for each point in the "grating" measurement was 1 second. All measurements were carried out under ambient conditions and at room temperature.

Results and discussion

Electrochemical surface functionalization of highly ordered pyrolytic graphite (HOPG) was carried out by cyclic voltammetry in aqueous solutions of the aryl diazonium compounds (1 mM). Detailed protocols are described in the experimental section.

Fig. 1 illustrates the electrochemical behavior of the HOPG substrate immersed in grafting electrolytes containing either 4-NBD (Fig. 1a) or 4-CBD molecule (Fig. 1b). In both cases, the first few cycles show broad, irreversible reduction peaks at around $E = +0.47$ V and $E = +0.27$ V *vs.* Ag/AgCl, respectively. These peaks are assigned to the reduction of the diazonium cations and the formation of the corresponding aryl radicals, which attack either the HOPG surface directly or the grafted molecules.[2,19,32] The difference in the reduction potentials of the aryl diazonium cations is because of their LUMO energy levels (Table S1†). Meanwhile, the second cycles are featureless, indicating a surface blocking effect by the grafted layer formed during the first cycle. The detailed mechanism describing the reduction and grafting process under electrochemical control can be found elsewhere.[19,32]

The quality of the films grafted on HOPG is characterized by cyclic voltammetry (CV), as shown in Fig. 1c, including the CVs of bare HOPG and HOPG grafted by 4-NBD or 4-CBD in 1 mM $K_3Fe(CN)_6$. For bare HOPG, a quasi-reversible redox pair of peaks is observed (black curve) centered at $E_f = +0.2$ V *vs.* Ag/AgCl, with a peak separation of 80 mV. This confirms free charge transfer throughout the electrolyte-HOPG interface.

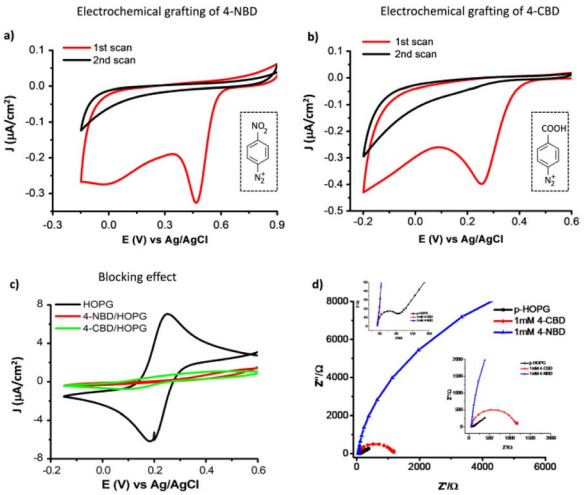

Fig. 1 First two voltammetric cycles of HOPG in (a) 1 mM 4-NBD + 50 mM HCl, (b) 1 mM 4-CBD + 50 mM HCl + excess $NaNO_2$; (c) cyclic voltammograms of bare HOPG (black curve), functionalized HOPG after electrochemical grafting of 1 mM 4-NBD (red curve), and 1 mM 4-CBD (green curve), in 1 mM $K_3Fe(CN)_6$ + 0.2 M Na_2SO_4 electrolyte; scan rate: 50 mV s^{-1}; (d) Nyquist plots for electrochemical impedance spectroscopy of an HOPG electrode (black curve), HOPG electrodes modified with 1 mM 4-CBD (green curve), and 1 mM 4-NBD (red curve). The measurements were performed at 10 mV in the frequency range from 10 kHz to 10 mHz.

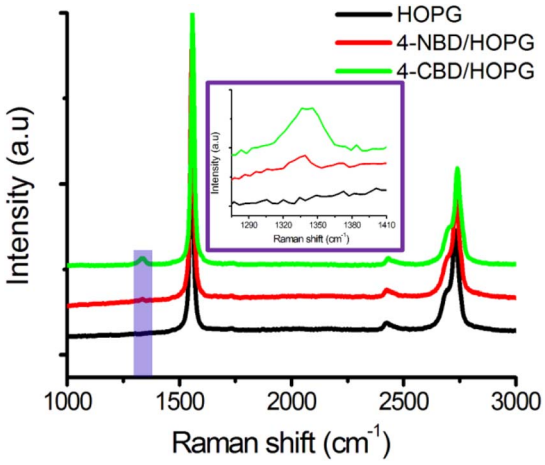

Fig. 2 Raman spectra of pristine HOPG (black curve), 4-NBD grafted HOPG (red curve), and 4-CBD grafted HOPG from 1 mM solutions, respectively. The spectra were averaged over 5 sample spots. Integration time 100 s.

After being grafted by either 4-NBD or 4-CBD aryl radicals, the redox current is almost completely blocked (red and green curves). This observation indicates that the HOPG surface is fully covered by non-conducting polyaryl layers.[36,37] Based on this comparison, the successful formation of the polyaryl layers grafted by either 4-NBD or 4-CBD molecules is demonstrated. Our results are supported by previous works reporting on the grafting of 4-NBD and 4-CBD using XPS to record the signature of the functional groups grafted.[19,20,23,38] These studies provided convincing data on the number of layers of 4-NBD and 4-CBD grafted onto graphitic surfaces and their bonding nature.

The electrical properties of pristine HOPG and diazonium-modified HOPG electrodes were also investigated using electrochemical impedance spectroscopy measured in a 1 mM $K_3Fe(CN)_6$ + 0.2 M Na_2SO_4 electrolyte, as shown in Fig. 1d. The charge transfer resistances of individual electrodes correspond to the diameter of the semicircles in the Nyquist plot. With respect to pristine HOPG, the charge transfer resistance is small due to its conductive nature (black curves). A higher value of the charge transfer resistance compared to pristine HOPG is recorded for the 4-CBD/HOPG electrode (green curves). In contrast, the 4-NBD/HOPG electrode shows an apparently large charge transfer resistance (red curves).

Raman spectroscopy is used to characterize the extent of covalent functionalization as it discloses information related to surface defects formed on carbon surfaces. Based on the integrated intensity ratio of the D- and G-peaks (I_D/I_G), it is possible to determine the surface density of the grafted molecules.[39,40] Fig. 2 compares Raman spectra before (black curve) and after grafting by 4-NBD (red curve) and 4-CBD (green curve). All Raman spectra are averaged over five sample spots. The Raman spectrum of bare HOPG shows typical peaks at 1576 and 2679 cm^{-1}, which are assigned to the G-band and 2D-band, respectively.[19] We did not observe any D-band peak, indicating that the HOPG surface is defect free. After introducing the HOPG surface to the electrografting process with either 4-NBD or 4-CBD electrolytes, apart from the two characteristic peaks of the pristine HOPG surface, additional features at 1336 cm^{-1} (red curve) and 1341 cm^{-1} (green curve) appear for 4-NBD and 4-CBD, respectively. These peaks are assigned to the D-band, which is only activated upon the presence of structural disorder in the sp^2 carbon lattice.[41] The D-band intensity caused by the grafting of 4-NBD molecules is low ($I_D/I_G = 0.007$), indicating a very low number of sp^3 defects on the HOPG surface. More details can be found in previous work.[19,20] In comparison, the D-band intensity obtained with 4-CBD (I_D/I_G = 0.035) is higher at the same concentration conditions. These results imply that the molecular density of 4-CBD covalently grafted to the HOPG surface is higher than that of 4-NBD.

The surface morphology of the grafted HOPG samples was then analyzed by AFM, as shown in Fig. 3. The results indicate that the HOPG surface is fully covered by compact thin films. A closer look reveals that the top layer formed by 4-NBD radicals protrudes mushroom-like features (Fig. 3a and b)that are not observed with respect to the layer formed by 4-CBD (Fig. 3c and d). This suggests a difference in the film growth process between the two moieties. To determine the thickness of the grafted films, AFM tip-assisted scratching was performed to expose the HOPG surface. Fig. S1† shows the AFM images of both 4-NBD and 4-CBD grafted layers after being scratched, and the line profiles measured across the scratched areas. The thicknesses of the 4-NBD and 4-CBD grafted layers were found to be 3.3 nm and 3.4 nm, respectively (Fig. S1b and d†), indicating multilayer formation with both of them. This is consistent with previous reports.[19] These multilayers are formed by further attachment of the aryl radicals to the 3,5 positions of the grafted ones, resulting in the formation of the so-called "dendritic feature".[19,34] However, it is not possible to

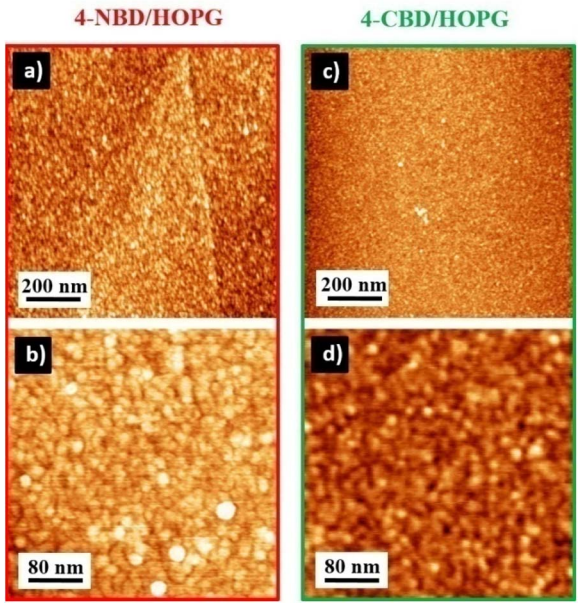

Fig. 3 AFM images showing surface morphologies of (a, b) 4-NBD and (c, d) 4-CBD covalently grafted to HOPG upon employing grafting electrolytes containing 1 mM corresponding diazonium salts.

differentiate the effect of the substituents on the formation of the grafted films because both molecules form multilayers under these experimental conditions. Therefore, a new approach involving the grafting of lower concentrations of the aryl diazoniums was employed to investigate the underlying differences.

Fig. 4 shows AFM images and line profiles (LPs) for samples grafted with 0.01 mM and 0.1 mM solutions, respectively, of 4-NBD and 4-CBD. The graphitic surface is randomly grafted by 4-NBD radicals at low concentration (0.01 mM). The root-mean-square (RMS) roughness is 0.81 nm.[33] The height of the bright features on the HOPG basal plane is 2.0 ± 0.2 nm (LP1), which is about 2.5 times higher than the height calculated for a vertically oriented nitrophenyl group (0.8 nm).[28] This indicates that polyaryl growth already occurs even at low coverage of 4-NBD species grafted onto the HOPG surface. This phenomenon becomes more evident by increasing the concentration of 4-NBD to 0.1 mM. At this point, the grafted HOPG surface is clearly inhomogeneous, and shows the formation of a porous/loosened multilayered structure (Fig. 4b). The height and RMS roughness of this grafted layer is 3.5 ± 0.2 nm (LP2) and 0.51 nm, respectively. This indicates that 4-NBD radicals react preferentially with already grafted aryl groups, thereby hindering aryl radicals grafting directly to the HOPG surface.

In contrast, high coverage of 4-CBD grafted onto the HOPG surface is recorded at a concentration of 0.01 mM (Fig. 4c). The average thickness of the grafted layer is about 1.1 ± 0.2 nm, similar to the molecular length of 4-CBD. This means that 4-CBD radicals tend to directly graft onto the HOPG surface rather than attacking the 3,5-positions of the 4-CBD grafted species. More interestingly, increasing the concentration of 4-CBD molecules leads to levelling of the first grafted layer, coupled with further growth of the second layer, as shown in Fig. 4d. Based on the line profile 4 (LP4), the thickness of the second grafted layer is similar to that of the first one, *i.e.*, also 1.1 ± 0.2 nm. Under these grafting conditions, 4-CBD radicals covalently bond to the HOPG surface in a layer-by-layer manner. Fig. S2† illustrates more detail on the nucleation and growth of the second layer. Accordingly, 4-CBD radicals first anchor to the already grafted layer, nucleating tiny dish-like features. Subsequently, these merge and form bigger features until the whole surface is covered. Thus, the layer-by-layer growth occurs for longer deposition times or higher concentration of 4-CBD precursor. This behavior is clearly different from the grafting process of 4-NBD moieties.

AFM imaging only serves to visualize the film morphology without providing a quantitative evaluation of the density of covalently anchored sites due to its limited spatial resolution. Therefore, scanning tunnelling microscopy (STM), a surface imaging technique that probes the local density of states (LDOS) with atomic resolution, was used to determine the density of grafted molecules, in real space. Fig. 5 presents STM images of

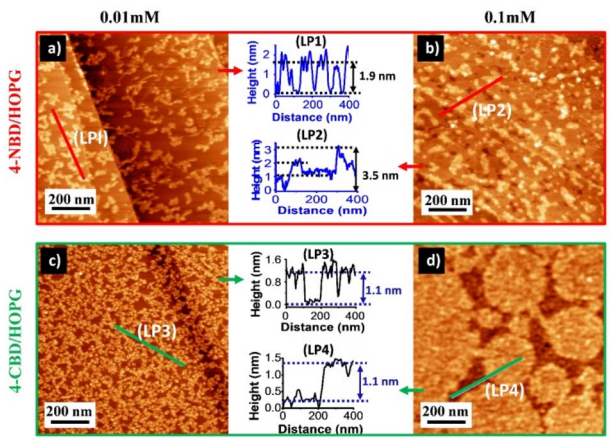

Fig. 4 AFM images illustrating surface morphology difference of (a, b) 4-NBD and (c, d) 4-CBD covalently grafted to HOPG surface by using 0.01 mM and 0.1 mM corresponding diazonium salts.

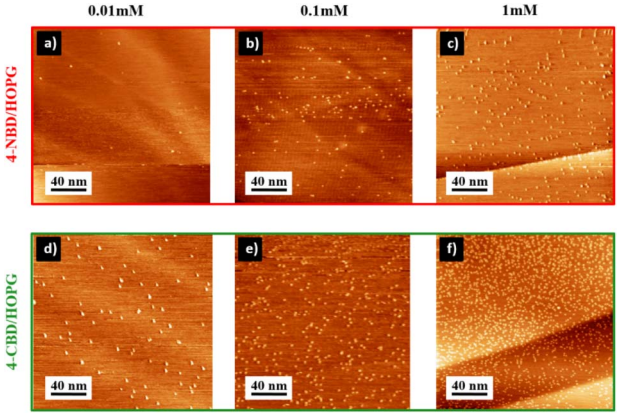

Fig. 5 Ambient STM images of HOPG surfaces exposed to various concentrations of 4-NBD (a–c) and 4-CBD (d–f). Measuring parameters for image (a–c): $V_s = -0.700$ V, $I_t = 80$ pA and (d–f): ($V_s = -0.700$ V, $I_t = 100$ pA).

HOPG surfaces covalently grafted by 4-NBD and 4-CBD with various concentrations.

Despite the fact that the density of bright features is generally proportional to the concentration of the grafting solutions used for both cases, there are significant differences. Specifically, the density of 4-CBD grafted to HOPG is obviously higher than that of 4-NBD. For instance, while the density of 4-NBD grafted species at a concentration of 1 mM is approximately 0.01 per nm^2,[19] the corresponding value for 4-CBD is as high as 0.06 per nm^2 under the same experimental conditions. The STM observations are in line with the AFM results. Due to the propensity for multilayered formation, the HOPG surface is shadowed by the dendritic features, resulting in a restriction of the density of 4-NBD radicals that can directly graft onto the HOPG surface. In contrast, the density of 4-CBD is detectably high due to the layer-by-layer growth mechanism, which supports a fully formed first layer prior to the formation of a second layer.

Discussion

Both employed aryl radicals have shown to covalently functionalize graphite surfaces successfully as revealed by AFM, STM and Raman spectroscopy. Although having a low steric hindrance, they behaved in two distinct grafting mechanisms for multilayer formation.

In the case of 4-NBD, dendritic growth was observed for all concentrations used. At a concentration of 0.01 mM, the HOPG surface was still fully available for further grafting of 4-NBD molecules, which nevertheless preferably attacked the already grafted molecules, resulting in the formation of a multilayer. This tendency became more apparent at higher concentrations of 4-NBD, as shown in Fig. 4a and b. The AFM visualization was further supported by STM results, which showed a very low density of 4-NBD molecules directly grafted onto the HOPG surface (Fig. 5a–c). This is in line with the low D-band intensity observed in the Raman spectrum for 4-NBD. In contrast to 4-NBD, a layer-by-layer mechanism was observed for 4-CBD molecules. At a low concentration (0.01 mM), a sub-monolayer was observed (Fig. 4c and 5d). At a concentration of 0.1 mM, the second layer growth became evident, as seen in the formation of "dish-like" features on the first grafted layer (Fig. 4d and 5e). Thus, the density of 4-CBD directly grafted onto the HOPG surface, calculated at 0.06 grafted species per nm^2, is significantly higher than that observed for 4-NBD at the same concentration.

Despite the fact that the number of factors involved in the film growth process has not been concluded yet, the differences in the growth mechanisms between 4-NBD and 4-CBD grafting can probably be interpreted by a combination of the following plausible main reasons: (i) the steric effect, and (ii) the electronic nature of the substituents.

Taking into account the molecular sizes of the substituents, it can be rationalized that the size of the nitro (NO_2) functional group, calculated by the van der Waals radii, is approximately 2.4 Å, which is half the size of the aryl ring.[42] Therefore, the *ortho* positions of the aryl ring are not shielded by the NO_2 substituent, causing a further attachment of as-reduced aryl radicals to the 3,5-positions of the grafted phenyl rings, resulting in dendritically multilayered formation, which favors radical polymerization.[43] In contrast, the carboxyl (COOH) functional groups are significantly larger (3.8 Å) than the NO_2 group and can partially shield the 3,5-positions of the phenyl rings.[43] Consequently, the multilayered formation is disfavored, since the multilayer growth *via* nucleophilic attack is sterically hindered.[44,45] Therefore, these aryl radicals are prone to directly attach to the HOPG surface, thereby increasing the grafting efficiency of 4-CBD in comparison with 4-NBD.

The electronic nature of the substituents is also considered a key factor influencing the growth rate and thickness of the grafted layers, particularly in relation to the so-called "non-radical mechanism" in layer formation.[43] Due to its electron-withdrawing nature, the NO_2 group is well-known as a strongly deactivating group for aryl substitution, resulting in a favorable polymerization by electrophilic attack of diazonium ions on grafted groups to form dendritic multilayers.[43,46,47] This is consistent with our observation of the 4-NBD moiety.

The superior grafting efficiency of 4-CBD in comparison to 4-NBD can be attributed to the electronic activation effect. The carboxy (COOH) group, as opposed to the NO_2 group, is a moderately deactivating group for electrophilic addition, which hinders the reaction between the pre-grafted species and reduced diazonium radicals.[43] This likely facilitates the direct attachment of aryl radicals to the HOPG surface, resulting in a higher grafting concentration, as supported by STM and Raman results. Hence, the variation in the activation effect of the aromatic ring positions can account for the observed discrepancy in layer growth between 4-NBD and 4-CBD.

Another plausible factor is the different reaction rates of the reactants to HOPG.[48] The SOMO energy level of the 4-CBD radical is relatively close to the Fermi level of HOPG compared to that of 4-NBD (Table S2†).[49,50] Thus, the aryl radicals formed from 4-NBD attack favorably to the grafted species rather than the HOPG surface.

Conclusions

It has been demonstrated that the covalent multilayer formation generated by diazonium chemistry strongly depends on the substituent's nature. This was visualized using a combination of cyclic voltammetry, Raman spectroscopy, and scanning probe microscopy methods such as atomic force microscopy, and scanning tunnelling microscopy. The multilayer formation of 4-NBD occurs *via* a dendritic growth mechanism, whereas 4-CBD multilayers are formed layer-by-layer. These results confirm the role of the functional group substituted in the 4-position on the arene ring on multilayer formation. These findings contribute in controlling the degree of functionalization of graphene and other 2D materials.

Author contributions

T. M. T. H. and T. H. P. designed and conducted all experiments. T. M. T. H. analyzed all measurement data. T. M. T. H. and T. H. P. wrote the manuscript. All authors discussed the results and revised the manuscript.

Conflicts of interest

The authors declare that we have no competing financial interests or personal relationships that could have appeared to influence the work reported in this paper.

Acknowledgements

This research is funded by Vietnam National Foundation for Science and Technology Development (Nafosted) under grant number 103.99-2020.65. SDF thanks the support of KU Leuven, *via* grant C14/19/079, and FWO, *via* grant G0DAW23N and G0A3220N.

References

1 N. Xin, *et al.*, Concepts in the design and engineering of single-molecule electronic devices, *Nat. Rev. Phys.*, 2019, **1**, 211–230.
2 H. Chen and J. Fraser Stoddart, From molecular to supramolecular electronics, *Nat. Rev. Mater.*, 2021, **6**, 804–828.
3 D. Kwong Hong Tsang, T. J. Lieberthal, C. Watts, *et al.*, Chemically functionalised graphene fet biosensor for the label-free sensing of exosomes, *Sci. Rep.*, 2019, **9**, 13946.
4 J. Wang, *et al.*, Linkage effect in the heterogenization of cobalt complexes by doped graphene for electrocatalytic CO_2 reduction, *Angew. Chem., Int. Ed.*, 2019, **58**, 13532–13539.
5 C. B. Huang, *et al.*, Molecule–graphene hybrid materials with tunable mechanoresponse: highly sensitive pressure sensors for health monitoring, *Adv. Mater.*, 2019, **31**, 1804600.
6 A. Bakandritsos, *et al.*, Covalently functionalized graphene as a supercapacitor electrode material, *FlatChem*, 2019, **13**, 25–33.
7 L. Wang, *et al.*, Conjugated molecule functionalized graphene films for energy storage devices with high energy density, *Electrochim. Acta*, 2020, **340**, 135804.
8 Y. Qin, *et al.*, Anthraquinone-functionalized graphene framework for supercapacitors and lithium batteries, *Ceram. Int.*, 2020, **46**, 15379–15384.
9 J. Zhang, *et al.*, Organic small molecule activates transition metal foam for efficient oxygen evolution reaction, *Adv. Mater.*, 2020, **32**, 1906015.
10 F. Niu, *et al.*, Hybrid photoelectrochemical water splitting systems: from interface design to system assembly, *Adv. Energy Mater.*, 2020, **10**, 1900399.
11 K. S. Mali, *et al.*, Nanostructuring graphene for controlled and reproducible functionalization, *Nanoscale*, 2015, **7**, 1566–1585.
12 S. Bouchareb, *et al.*, Non-covalent functionalization of graphene oxide using self-assembly of silver-triphenylphosphine for bactericidal formulations, *Mater. Chem. Phys.*, 2020, **243**, 122598.
13 A. Lopez and J. Liu, Covalent and noncovalent functionalization of graphene oxide with dna for smart sensing, *Adv. Intell. Syst.*, 2020, **2**, 2000123.
14 P. Zhang, *et al.*, Covalently functionalized graphene towards molecular-level dispersed waterborne polyurethane nanocomposite with balanced comprehensive performance, *Appl. Surf. Sci.*, 2019, **471**, 595–606.
15 T. M. T. Huynh, T. H. Phan and S. De Feyter, Surface engineering of graphite and graphene by viologen self-assembling: from global to local architectures, *J. Phys. Chem. C*, 2022, **126**, 6413–6419.
16 T. M. T. Huynh, *et al.*, Doping of graphene *via* adlayer formation of electrochemically reduced dibenzyl viologen, *J. Mater. Chem. C*, 2022, **10**, 2696–2702.
17 C. Wetzl, A. Silvestri, M. Garrido, H.-L. Hou, A. Criado and M. Prato, The covalent functionalization of surfacesupported graphene: an update, *Angew. Chem., Int. Ed.*, 2023, **62**(6), e202212857.
18 P. C. Mondal, Optical and electrochemical properties of covalent assembled bis(4′-carboxylic phenyl terpyridyl) Ru(II)-monolayer, *New J. Chem.*, 2015, **39**, 7403–7408.
19 J. Greenwood, T. H. Phan, *et al*, Covalent modification of graphene and graphite using diazonium chemistry: tunable grafting and nanomanipulation, *ACS Nano*, 2015, **9**, 5520–5535.
20 T. H. Phan, *et al.*, Graphite and graphene fairy circles: a bottom-up approach for the formation of nanocorrals, *ACS Nano*, 2019, **13**, 5559–5571.
21 G. Ambrosio, *et al.*, Interface chemistry of graphene/cu grafted by 3,4,5-tri-methoxyphenyl, *Sci. Rep.*, 2020, **10**, 4114.
22 Y. Xia, *et al.*, Grafting ink for direct writing: solvation activated covalent functionalization of graphene, *Adv. Sci.*, 2022, **9**, 2105017.
23 K. Boukerma, M. M. Chehimi, J. Pinson and C. Blomfield, X-ray Photoelectron spectroscopy evidence for the covalent bond between an iron surface and aryl groups attached by the electrochemical reduction of diazonium salts, *Langmuir*, 2003, **19**, 6333.
24 J. Pinson and F. Podvorica, Attachment of organic layers to conductive or semiconductive surfaces by reduction of diazonium salts, *Chem. Soc. Rev.*, 2005, **34**, 429–439.
25 J. Ru, B. Szeto, A. Bonifas and R. L. McCreery, Microfabrication and integration of diazonium-based aromatic molecular junctions, *ACS Appl. Mater. Interfaces*, 2010, **2**(12), 3693–3701.
26 J. C. Lacroix, G. Trippe-Allard, J. Ghilaneand and P. Martin, Electrografting of conductive oligomers and polymers using diazonium electroreduction, *Adv. Nat. Sci.: Nanosci. Nanotechnol.*, 2015, **5**, 015001.
27 A. Adenier, *et al.*, Formation of polyphenylene films on metal electrodes by electrochemical reduction of benzenediazonium salts, *Chem. Mater.*, 2006, **18**, 2021–2029.
28 P. A. Brooksby and A. J. Downard, Electrochemical and atomic force microscopy study of carbon surface modification *via* diazonium reduction in aqueous and acetonitrile solutions, *Langmuir*, 2004, **20**, 5038–5045.
29 C. Saby, B. Ortiz, G. Y. Champagne and D. Bélanger, Electrochemical modification of glassy carbon electrode using aromatic diazonium salts. 1. Blocking effect of 4-

nitrophenyl and 4-carboxyphenyl groups, *Langmuir*, 1997, **13**, 6805–6813.

30 P. Doppelt, G. Hallais, J. Pinson, F. Podvorica and S. Verneyre, Surface modification of conducting substrates. existence of azo bonds in the structure of organic layers obtained from diazonium salts, *Chem. Mater.*, 2007, **19**, 4570–4575.

31 T. Menanteau, *et al.*, Electrografting *via* diazonium chemistry: the key role of the aryl substituent in the layer growth mechanism, *J. Phys. Chem. C*, 2016, **120**, 4423–4429.

32 K. Tahara, *et al.*, Steric and electronic effects of electrochemically generated aryl radicals on grafting of the graphite surface, *Langmuir*, 2019, **35**, 2089–2098.

33 X. Zhang, *et al.*, Influence of the Para-substituents of benzene diazonium salts and the solvent on the film growth during electrochemical reduction, *Z. fur Phys. Chem.*, 2014, **228**, 557–573.

34 S. Phal, *et al.*, Electrografting of 4-Carboxybenzenediazonium on Glassy Carbon Electrode: The Effect of Concentration on the Formation of Mono and Multilayers, *Molecules*, 2020, **25**, 4575.

35 I. Horcas, *et al.*, WSXM: a software for scanning probe microscopy and a tool for nanotechnology, *Rev. Sci. Instrum.*, 2007, **78**, 013705.

36 J. Lehr, B. E. Williamson and A. J. Downard, Spontaneous grafting of nitrophenyl groups to planar glassy carbon substrates: evidence for two mechanisms, *J. Phys. Chem. C*, 2011, **115**, 6629–6634.

37 T. M. T. Huynh, *et al.*, Nanoconfined self-assembly on a grafted graphitic surface under electrochemical control, *Nanoscale*, 2017, **9**, 362–368.

38 L. Gillan, T. Teerinen, L. S. Johansson and M. Smolander, Controlled diazonium electrodeposition towards a biosensor for C-reactive protein, *Sens. Int.*, 2021, **2**, 100060.

39 Q. H. Wang, *et al.*, Understanding and controlling the substrate effect on graphene electron-transfer chemistry *via* reactivity imprint lithography, *Nat. Chem.*, 2012, **4**, 724–732.

40 S. Niyogi, *et al.*, Spectroscopy of covalently functionalized graphene, *Nano Lett.*, 2010, **10**, 4061–4066.

41 L. M. Malard, *et al.*, Raman spectroscopy in graphene, *Phys. Rep.*, 2009, **473**, 51–87.

42 A. Bondi, van der Waals volumes and radii, *J. Phys. Chem.*, 1964, **68**, 441–451.

43 T. Breton, E. Levillain, T. Menanteau and A. J. Downard, Evidence of monolayer formation from diazonium grafting with radical scavenger: electrochemical, AFM and XPS monitoring, *Phys. Chem. Chem. Phys.*, 2015, **17**, 13137.

44 X. Zhang, F. Rösicke, V. Syritski, *et al.*, Influence of the para-substitutent of benzene diazonium salts and the solvent on the film growth during electrochemical reduction, *Z. Phys. Chem.*, 2014, **228**, 557–573.

45 C. Combellas, D. Jiang, F. Kanoufi, J. Pinson and F. I. Podvorica, Sterically hindered diazonium salts for the grafting of a monolayer on metals, *Langmuir*, 2009, **25**, 286.

46 A. Mesnage, *et al.*, Spontaneous grafting of diazonium salts: chemical mechanism on metallic surfaces, *langmuir*, 2012, **28**, 11767–11778.

47 C. F. Olguín, *et al.*, Tuning the covering on gold surfaces by grafting amino-aryl films functionalized with Fe(ii) phthalocyanine: performance on the electrocatalysis of oxygen reduction, *Molecules*, 2021, **26**, 1631.

48 I. Fleming, *Radical Reactions. Frontier orbitals and organic chemical reactions*, John Wiley & Sons, United Kingdom, 2009, pp. 275–298.

49 B. Feuerbacher and B. Fitton, Experimental investigation of photoemission from satellite surface materials, *J. Appl. Phys.*, 1972, **43**, 1563–1572.

50 D. Liu, M. He, C. Huang, X. Sun and B. Gao, Fermi level dependence of chemical functionalization of graphene with benzoyl peroxide, *J. Phys. Chem. C*, 2017, **121**, 10546–10551.